ELSEVIER

Journal of Structural Geology 26 (2004) 1447–1464

JOURNAL OF STRUCTURAL GEOLOGY

www.elsevier.com/locate/jsg

Superposed buckle folding in the eastern Iberian Chain, Spain

José L. Simón

Departamento de Geología, Universidad de Zaragoza, 50009 Zaragoza, Spain

Received 29 January 2003; received in revised form 4 November 2003; accepted 15 November 2003

Available online 5 March 2004

Abstract

The Aliaga area (eastern Iberian Chain) shows large-scale examples of buckle superposition developed during Tertiary folding. In most cases, ENE-trending folds overprint earlier NNW–SSE-trending ones. The resulting structures are mapped, analysed, and genetically classified by comparison with analogue models described by several authors. The following types are found: standard Type 1 (1a: dome-and-basin structure, 1b: unequal-wavelength overprinted folds); modified Type 1 (1c: T-shaped 'joined' folds; 1d: T-shaped 'abutting' folds; 1e: L-shaped folds; 1f: 'snake-like' folds); standard Type 2 (2a: non-cylindrical buckling of earlier axial surfaces involving hinge replacement). Different superposed sets of flexural-slip striations record successive folding episodes in snake-like folds, and hinge replacement in the case of Type 2a superpositions. Types 1 and 2 apparently develop where the earlier folds have interlimb angles over and below 90°, respectively, which fits the results of analogue modelling and theoretical analysis by previous authors. Types 1b and 1d are associated with higher W1/W2 wavelength ratios than Types 1a and 1c. Other controlling factors are viscosity contrast and erosion processes. Specifically, erosion of competent limestone beds in the hinge zone of a NNW–SSE-trending anticline allowed the near-vertical eastern limb to be refolded into snake-like folds.

Keywords: Superposed buckling; Fold interference; Iberian Chain; Spain

1. Introduction

In superposed buckle folding, the first generation folds do not refold as passive planes or lineations. On the contrary, the former have an overriding influence on the mechanical development of second generation folds, controlling their geometry and axial orientation (Tobisch, 1967; Ghosh, 1970; Skjernaa, 1975; Watkinson, 1981; Ghosh et al., 1993; Grujic, 1993). The classic interference models proposed by Ramsay (1967) involve passive or shear folding, so they do not necessarily explain buckle superposition.

The approach to the geometry and kinematics of superposed buckle folding has been mainly analytical (Ramsay, 1967; Ghosh, 1970; Grujic, 1993) and experimental (Ghosh and Ramberg, 1968; Skjernaa, 1975; Ghosh et al., 1992, 1993, 1995, 1996). Unfortunately, most of these theoretical and analogue models do not refer to actual field examples. Regional studies describing and analysing superposed buckle folds are few. Julivert and Marcos (1973), Aller and Gallastegui (1995) and Alvarez-Marrón (1995) described interference patterns between folds parallel to the arched thrusts of the Cantabrian zone (northern Spain) and another younger radial buckle fold set, in which both Types 1 and 2 of Ramsay (1967) coexist. Skjernaa (1975), Watkinson (1981) and Roy et al. (1998) show small-scale examples of Type 1 superposition in environments of moderate to high deformation (so not strictly representative of buckle folding). Liesa (2000) describes an example of gentle Type 1 superposed folds in Sierra del Pobo (central-eastern Iberian Chain, some 20 km west of Aliaga).

The Aliaga area, located near the northeastern boundary of the Iberian Chain (eastern Spain), shows very conspicuous and spectacular examples of buckle superposition developed during Tertiary compression. They were identified and briefly described many years ago, but the work was published only as a short paper in Spanish (Simón, 1980). Then, their images were widely diffused thanks to the cover of a textbook (Lisle, 1988) and to diverse initiatives for protection of the geological heritage (Geological Park of Aliaga, *European Geoparks* network).

The present paper provides a description and detailed kinematic analysis of the varied inventory of superposed folds found in this area. The work deals mainly with

E-mail address: jsimon@unizar.es (J.L. Simón).

0191-8141/$ - see front matter © 2004 Elsevier Ltd. All rights reserved.
doi:10.1016/j.jsg.2003.11.026

map-scale structures (orders of magnitude: 10^2–10^3 m in wavelength, 10^3–10^4 in axial length), which have been systematically mapped, described and analysed from aerial photographs and field surveys. Then they have been classified by comparison with published analogue models. A few minor second generation folds have been analysed on selected outcrops in order to obtain complementary data on flexural-slip kinematics, but no example of small-scale buckle superposition (both first and second generation fold wavelengths under 10^2 m) was found in the region. So, the eventual occurrence of the different combinations predicted by Ghosh et al. (1993) in superposed buckling of two orders of folds could not be explored.

2. Geological setting

The Iberian Chain is an intraplate mountain range, oblique to the northern (Pyrenean) and southern (Betic) active margins of the Iberian Plate (Fig. 1b). It developed by inversion of the extensional Mesozoic Iberian basin, caused by compression both normal (NNE–NE) and parallel (SE–SSE) to its boundaries (Simón, 1986; Liesa, 2000; Capote et al., 2002). The main, NNE–NE compression (Middle Eocene to Late Oligocene in age) was responsible for the principal folds and thrusts. The SE–SSE compression was mainly active during the Early Miocene, as the convergence between Europe and Africa was transferred from the Pyrenean to the Betic margin of Iberia, though it formed few new macrostructures.

The Aliaga area is located within the Maestrazgo sector in the eastern Iberian Chain (Fig. 1). Its compressional architecture is controlled by the contrasting behaviour of the Palaeozoic basement and the Mesozoic–Tertiary cover, separated by a regional detachment at the Middle–Upper Triassic lutites and evaporites (Guimerà, 1988). In the northern Maestrazgo, the cover is affected by a tight thrust-and-fold belt in which several sharp inflexions between NW–SE and NE–SW trends were induced by large late-Variscan, steeply dipping faults guiding basement deformation (Simón, 1984; Guimerà, 1988). NW–SE striking faults, such as those bounding the Calatayud–Montalbán

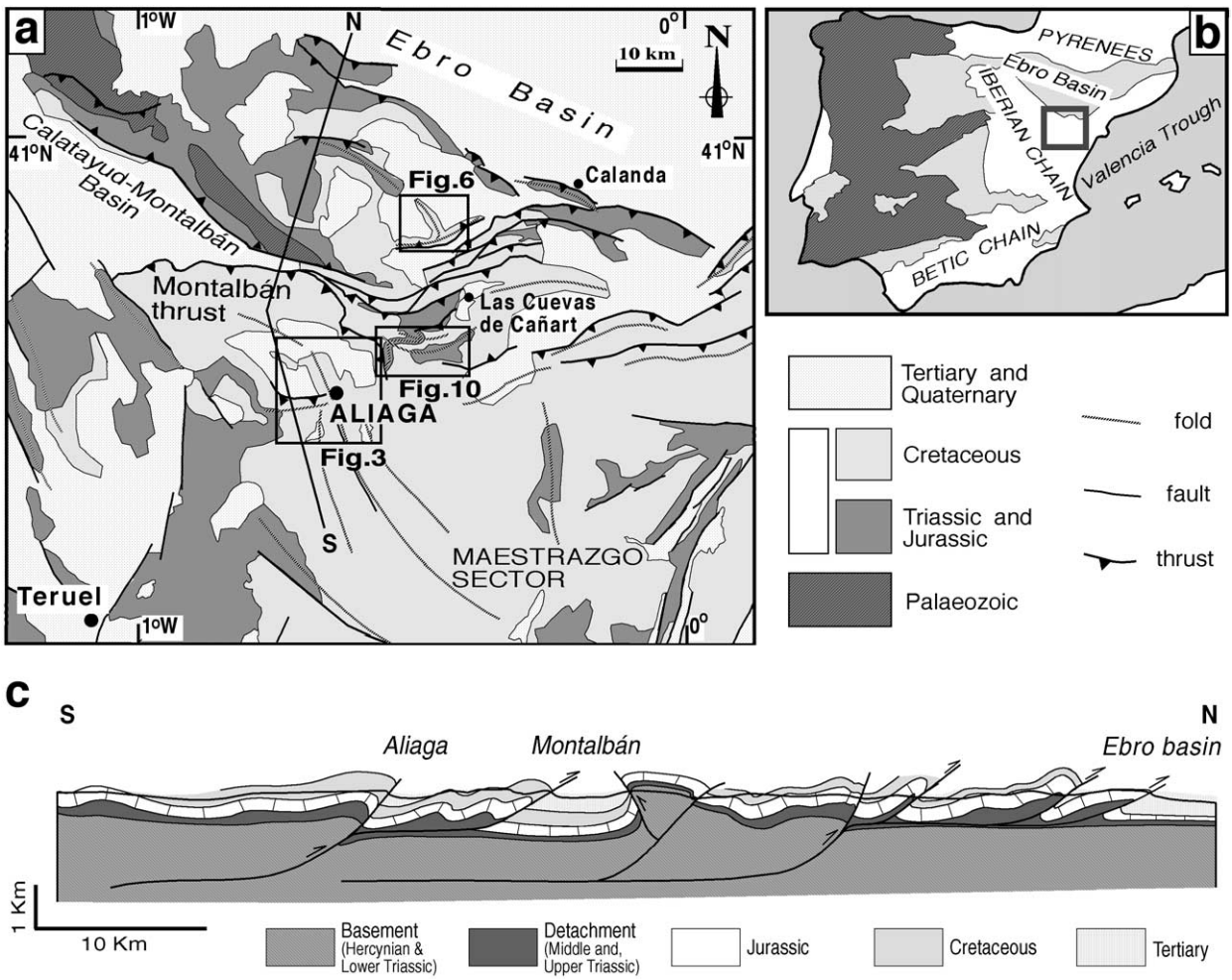

Fig. 1. Geological setting of the studied area. (a) Schematic map of the northeastern Iberian Chain, with location of the studied areas. (b) Location within the Iberian Peninsula. (c) Schematic cross-section.

basin (Fig. 1a), underwent reverse-dextral wrench movement, whereas NE–SW striking faults (Calanda–Aliaga) have sinistral movements.

The Mesozoic cover in Aliaga (about 2000 m thick) shows a stratigraphical succession (Fig. 2) characterized by alternating carbonate (marine) and siliciclastic (continental) sediments. The rheological model can be seen as a multilayer composed of three main carbonate, competent ensembles (Jurassic, Urgon facies, Upper Cretaceous) separated by two siliciclastic, less competent ensembles (Purbeck–Weald facies; Escucha and Utrillas formations). The latter behave as local detachment levels which favour disharmonic folding (Simón, 1980).

The studied area occupies the hanging wall of the Montalbán thrust (see Fig. 1a), displaced about 5–8 km

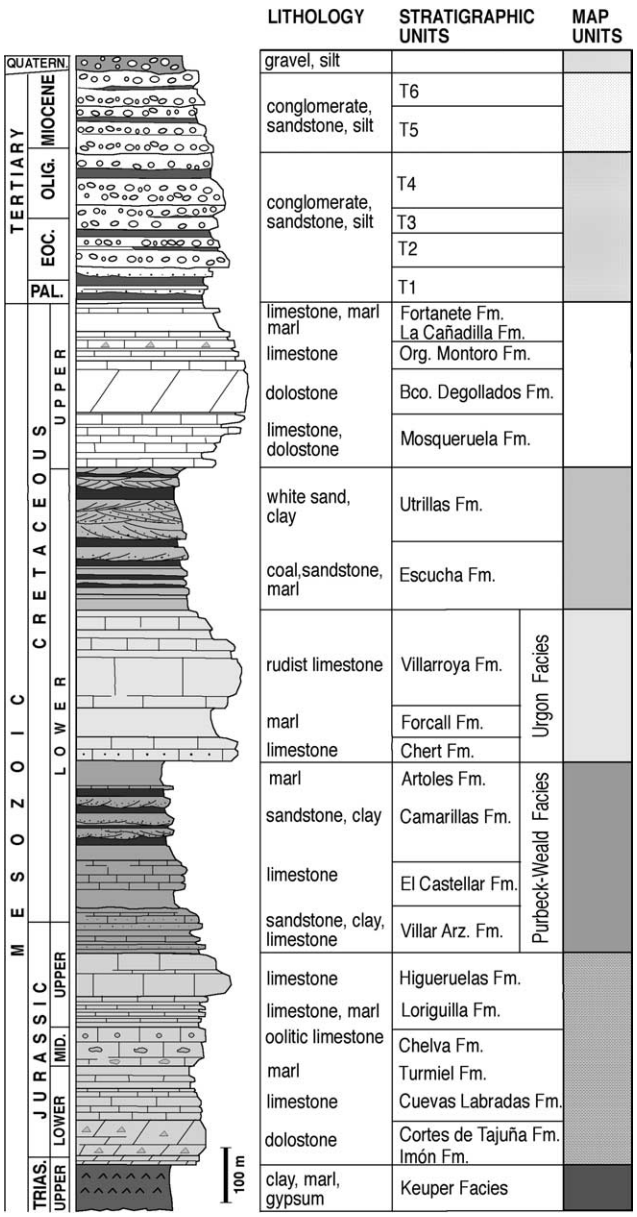

Fig. 2. Synthetic stratigraphic succession in the Aliaga area.

during the Oligocene and Early Miocene times (González and Guimerà, 1993; Casas et al., 2000), with successive transport directions towards the NNE and NNW (Liesa, 2000). At the same time, it was strongly deformed by abundant folds that can be grouped into two sets (Fig. 3). The first set is made up by NW–SE-trending folds (northern part of the thrust sheet), and a few long NNW–SSE- to N–S-trending folds (southern part): (a) the Campos–Miravete anticline, a box-shaped, 20-km-long fold that forms the spine of the zone; (b) the La Lastra syncline; (c) the Camarillas syncline. The ENE–WSW-trending folds are mostly concentrated within a narrow band on the latitude of Aliaga, which overprints and divides the Campos–Miravete anticline into two segments. They are accompanied by a number of thrusts parallel to them, the most important one being the Cobatillas thrust. A number of long-wavelength folds of both sets, such as the Campos–Miravete anticline and the overturned anticline associated with the Cobatillas thrust, are fault-propagation folds related to the positive inversion of inherited normal faults (Guimerà and Salas, 1996; Simón et al., 1998). The others (mainly those belonging to the second set) are essentially buckle folds detached either on the Middle–Upper Triassic or on incompetent Cretaceous levels. So, although their spatial distribution suggests the presence of a basement fault, each individual fold appears to have developed by a buckling mechanism.

As Tertiary folds grew, continental (mainly alluvial and lacustrine) sediments covered most of the northern half of the Aliaga area (Fig. 3), infilling a piggy-back basin transported on the Montalbán thrust sheet (Fig. 1). They can be grouped into six tectonosedimentary units (T1–T6; Fig. 2) bounded by unconformities related to successive compressive structures (González and Guimerà, 1993). In addition to other geometric and kinematic features, these tectonosedimentary relationships indicate that the ENE–WSW-trending folds at Aliaga are younger than the NNW–SSE ones, as will be discussed in detail in Section 5.

The landscape allows good observation of tectonic structures. These were cut by flat erosion surfaces during the Neogene, but the land underwent a new elevation by the Upper Pliocene giving rise to downcutting by the fluvial network. Selective erosion of hard and soft rocks allowed the fold interference structures to display clearly their 3-D geometry.

3. Classification systems of superposed buckle folds

Though the interference models defined by Ramsay (1967) cannot be strictly applied to buckle superposition, the essence of that classification, including the terminology, can be retained by using the modification proposed by Thiessen and Means (1980). According to these authors, four types can be differentiated depending on whether early

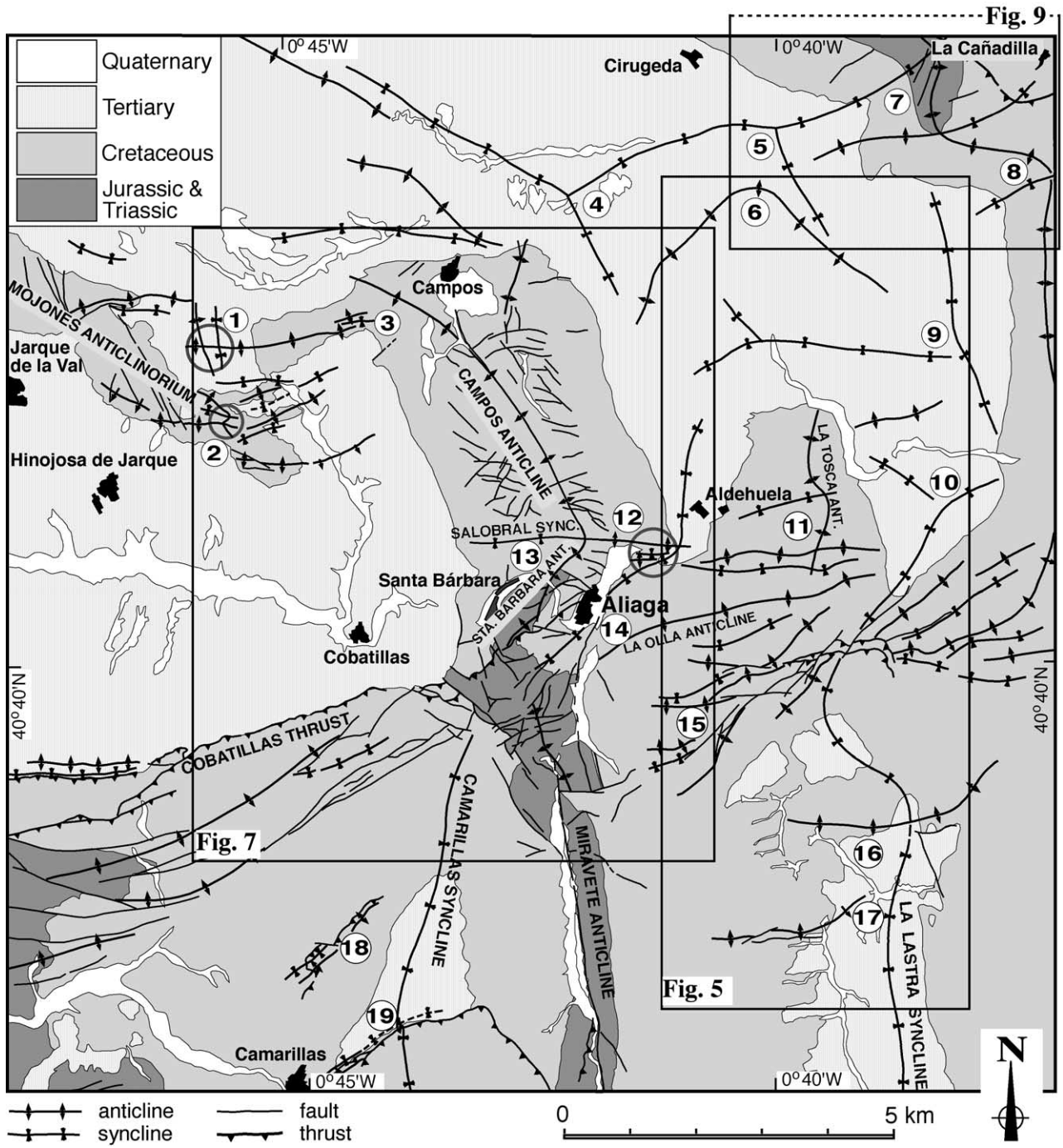

Fig. 3. Structural map of the Aliaga area. Numbers indicate location of the examples of superposed folding described in this paper. Type 1a: case 1. Type 1b: cases 8, 11, 16 and 19. Type 1c: cases 5(?) and 10(?). Type 1d: cases 3, 4(?), 9(?), 15, 17 and 18. Type 1e: case 6. Type 1f: cases 12 and 14. Type 2a: cases 2, 7 and 13.

hinge lines and axial planes remain straight and planar or become folded as a result of the second deformation:

	Earlier hinges	Earlier axial surfaces
Type 0	Straight	Planar
Type 1	Folded	Planar
Type 2	Folded	Folded
Type 3	Straight	Folded

Type 0 patterns, with the earlier folds that remain cylindrical and with axial surfaces that remain planar, can nevertheless be considered as a case of fold superposition since the final geometry (tightness and fold orientation) is a product of two deformations (Ghosh, 1993). Types 1–3 are the classical types defined by Ramsay (1967).

Ghosh and Ramberg (1968) and Skjernaa (1975) obtained two superposition types in the laboratory that are similar to Types 1 and 2 of the above classification:

- *First type*: The superposed folds do not distort the early axial surfaces except locally. Various geometries can form, including dome-and-basin geometry, showing a number of particularities: second-generation folds are consistently smaller than the early folds; they are generally less continuous and die out in a hinge of an early fold; in some cases they develop only on one limb of the early fold.
- *Second type*: This involves bending of the axial surfaces of the early folds, and refolding of originally sub-horizontal F_1 hinges within the horizontal plane. A late anticline on the limb of an early fold continues as a syncline on the other limb. These second-generation folds are usually conical and occupy roughly triangular areas on maps, showing steeply plunging axes. An F_2 antiform has a relatively wide span close to the F_1 antiformal hinge and it narrows down at the F_1 synformal hinge; F_2 synforms change in the opposite way. Second-type geometry appears as a consequence of maximum resistance offered by early hinge zones to a second deformation. Early hinges constitute a structural anisotropy that strengthens the material, owing to compatibility problems inherent to simultaneous refolding of both limbs (Ramsay, 1967, p. 548; Ramsay and Huber, 1987, p. 489; Johns and Mosher, 1996).

More recent theoretical and experimental models defined by Ghosh et al. (1992) divide Types 1 and 2 into four different 'modes' of superposed buckling:

- *First mode* ('Type 1a' in the nomenclature of the present paper, see Fig. 4): Classic dome and basin, Ramsay Type 1.
- *Second mode* ('Type 1b'): Small F_2 folds riding over larger F_1 folds, F_2 showing a shorter wavelength than that of F_1. This should be the common way of Type 1 superposition according to the analytical approach by Ghosh (1970), which demonstrates that the wavelength of buckle folds developed by compression parallel to the fold axes of a previously corrugated sheet is smaller than that which would have developed in a flat sheet.
- *Third mode* ('Type 2a'): Non-cylindrical F_2 folds bending F_1 hinges and axial planes. F_2 hinges usually plunge in opposite directions on both limbs of F_1 folds. The sinuous F_2 hinge is newly created by replacing the old F_1 hinge; this involves a difference with the Type 2 interference of Ramsay: what appears to be a strongly curved F_1 hinge is in reality a new feature developed under the second deformation.
- *Fourth mode* ('Type 2b'): Classic Ramsay Type 2 superposition without concomitant hinge replacement. F_2 synfomal and antiformal hinges usually plunge in the same direction.

4. Description and classification of superposed folds in the Aliaga area

Many buckle superposition structures mapped in the Aliaga area are analogous to published experimental models, whereas other ones are modified or variant types whose geometry and kinematics need further discussion (Fig. 4). Types 2b and 3 (classical Ramsay Types 2 and 3) do not appear within the studied region, but they have been included for completeness. Although the basis of this classification, as stated by Ramsay (1967) and Thiessen and Means (1980), is essentially geometrical, the different subtypes within Type 1 are defined using kinematic and genetic criteria in which timing and conditions of folding play a role.

4.1. Standard Type 1

The classic dome-and-basin structure (Type 1a, *First mode* of Ghosh et al. (1992)) was only observed at one site where very gentle N–S- and E–W-trending folds are found together. It is located to the north of Mojones anticlinorium (site 1 in Figs. 3 and 7a), where the western segment of the Loma del Villomar anticline interferes with two N–S-trending folds. The dome-and-basin structure is mainly observed in Tertiary deposits, with a small isolated outcrop of Upper Cretaceous limestones at the intersection of both orthogonal anticlines. The geometry alone does not define any overprinting relationship. Owing to the gentle amplitude of domes and basins, neither 'coaptation folds' (Stauffer, 1988) nor 'curvogenetic folds' necessary for preserving constant bed-length folding and isometric deformation (Lisle, 1992; Lisle et al., 1990) are associated with them.

Unequal-wavelength Type 1 superpositions (Type 1b, *Second mode* of Ghosh et al. (1992), see Fig. 4) are more abundant. They occur where tight, E–W-trending folds of middle-scale (usually hectometric) wavelength develop across the wide N–S-trending folds of Aliaga, especially on their near-flat crests or troughs. Since these second generation folds are true buckle folds (most of them detached on Lower Cretaceous clays and marls), their shorter wavelengths and higher tightness can be considered as significant features fitting the theory of Ghosh (1970). The following cases are the most conspicuous ones. (a) The zone east of Aldehuela, where several E–W folds overprint the crest of the box-shaped, N–S-trending La Tosca anticline (site 11 in Figs. 3 and 5). (b) The E–W-trending anticline riding over La Lastra syncline (site 16 in Figs. 3 and 5). (c) The overturned folds associated with the arched thrust at Camarillas (site 19 in Fig. 3), which are accompanied to the south (out of Fig. 3) by other E–W-trending folds all cutting the Camarillas syncline (Guimerà, 1988). (d) The right, tight syncline at Barranco de las Calzadas (site 8 in Figs. 3 and 9a), developed in special conditions that we will discuss later. Cases 8 and 16 show

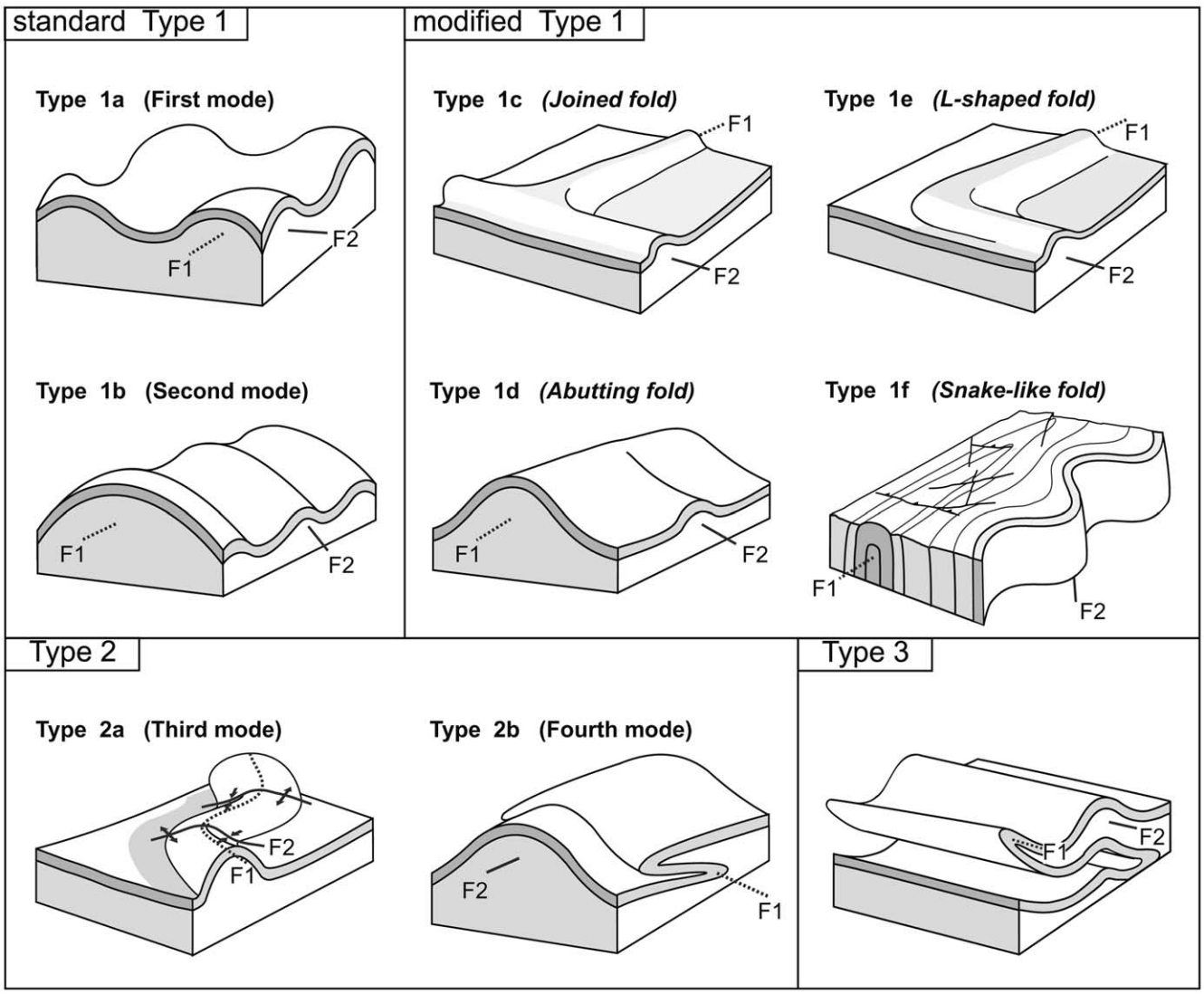

Fig. 4. Genetic classification of superposed buckle folds. '*First mode*', '*Second mode*', '*Third mode*', '*Fourth mode*': terms used by Ghosh et al. (1992). '*Joined fold*', '*Abutting fold*', '*Snake-like fold*': informal terms used in this paper. Types 1a, 2b and 3 are the classical interference models of Ramsay (1967). Types 2b and 3 have not been observed within the study area.

curved axial traces of the earlier folds that might be misinterpreted as Type 2. Nevertheless, their geometry does not fit Type 2: second generation folds are not conical and they do not change from anticline to syncline as they cross the earlier fold.

4.2. Modified Type 1

Special cases of Type 1 interference form where later folds do not exactly 'overprint' but 'join' or 'abut' the early fold hinges. Strictly speaking, they should not be considered as true 'fold superpositions' but 'fold juxtapositions', in which those early fold hinges may not even be deformed. This situation gives rise to composite structures, frequently showing 'T' or 'L'-shaped map patterns where an early fold and a later fold are welded together. 'T'-shaped patterns represent a geometrical model which is ambiguous from the genetic point of view. Regarding the relative timing of interfering folds, either 'joined' or 'abutting' folds can develop.

A '*joined*' *fold* (Type 1c, Fig. 4) is a younger fold attached to the extremity of an older fold with a different trend. The largest and most conspicuous example in the study area is located near Los Olmos (Fig. 6, see location in Fig. 1). Here a long E–W-trending anticline, associated with an overthrust, is joined to an older NNW–SSE-trending anticline, producing a T-shaped pattern. The axial trace of the NW–SE anticline curves towards the intersection point, which suggests that it formed prior to the E–W fold. Relationships between folds and Tertiary deposits (see Section 5) confirm this interpretation.

An '*abutting*' *fold* (Type 1d, Fig. 4) is a later, usually smaller fold that develops on the limb of an earlier fold and abuts its hinge zone. This is equivalent to one of the

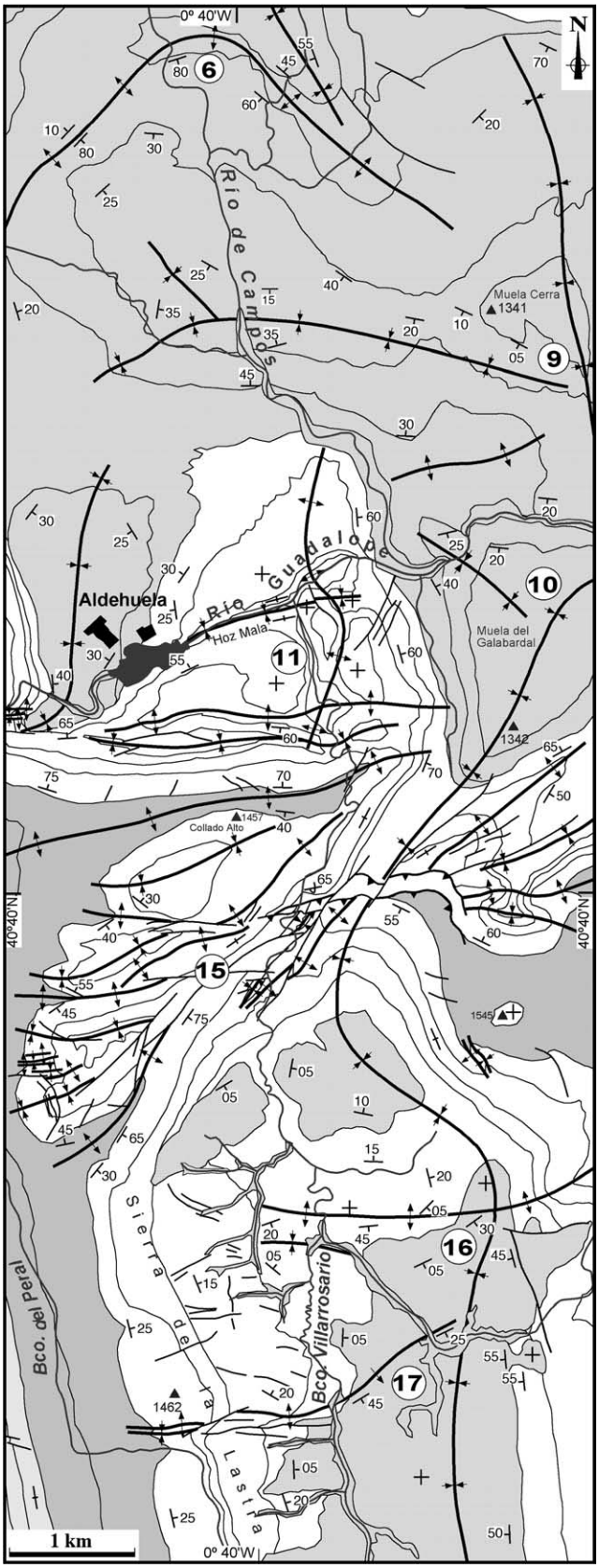

Fig. 5. Superposed folds east of Aliaga; see symbols for stratigraphic units in Fig. 2. Tertiary units mapped according to González (1989). Circled numbers: location of structures described in the text.

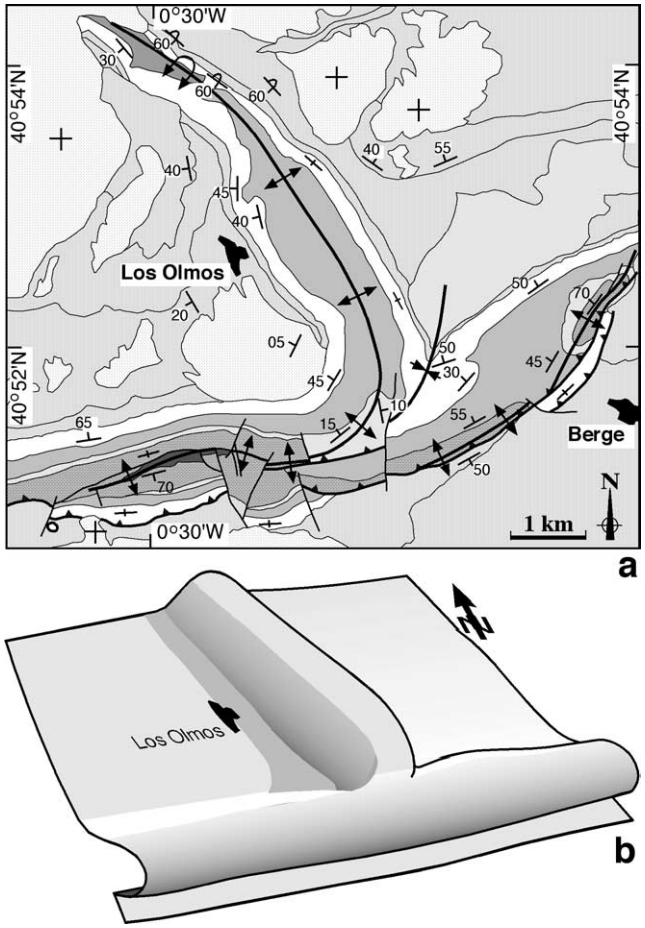

Fig. 6. Superposed folds at Los Olmos (Type 1c). (a) Geological map; see symbols for stratigraphic units in Fig. 2. Partially based on Marin et al. (1977). Tertiary units mapped according to González (1989); see location in Fig. 1. (b) 3D sketch of the overall structure (simplified reconstruction for the Cretaceous–Tertiary boundary).

'modified second mode' superpositions described by Ghosh et al. (1993) for buckled multilayers. Good examples of this type of interference were found on the western limbs of first-generation, NNW–SSE-trending folds: the La Lastra syncline (sites 15 and 17 in Figs. 3 and 5), the Campos anticline (site 3 in Figs. 3 and 7a), and the Camarillas syncline (site 18 in Fig. 3). In all cases the genetic interpretation of the final structure was based upon the general fold sequence inferred in the area.

'*L*'*-shaped folds* (Type 1e, Fig. 4) are also ambiguous in terms of time relationships, although in this case the geometrical model needs not to be divided into two different genetic types. In any case, this pattern should not be misinterpreted as Type 2 'crescent' or 'boomerang' pattern, in which both segments belong to a single first-generation fold (Skjernaa, 1975). The only example of L-shaped fold in our study area can be seen in Tertiary deposits NE of Aliaga (site 6 in Figs. 3 and 5).

'*Snake-like*' *folds* (Type 1f, Fig. 4) are cylindroidal, nearly vertical-axis folds which are abundant in the

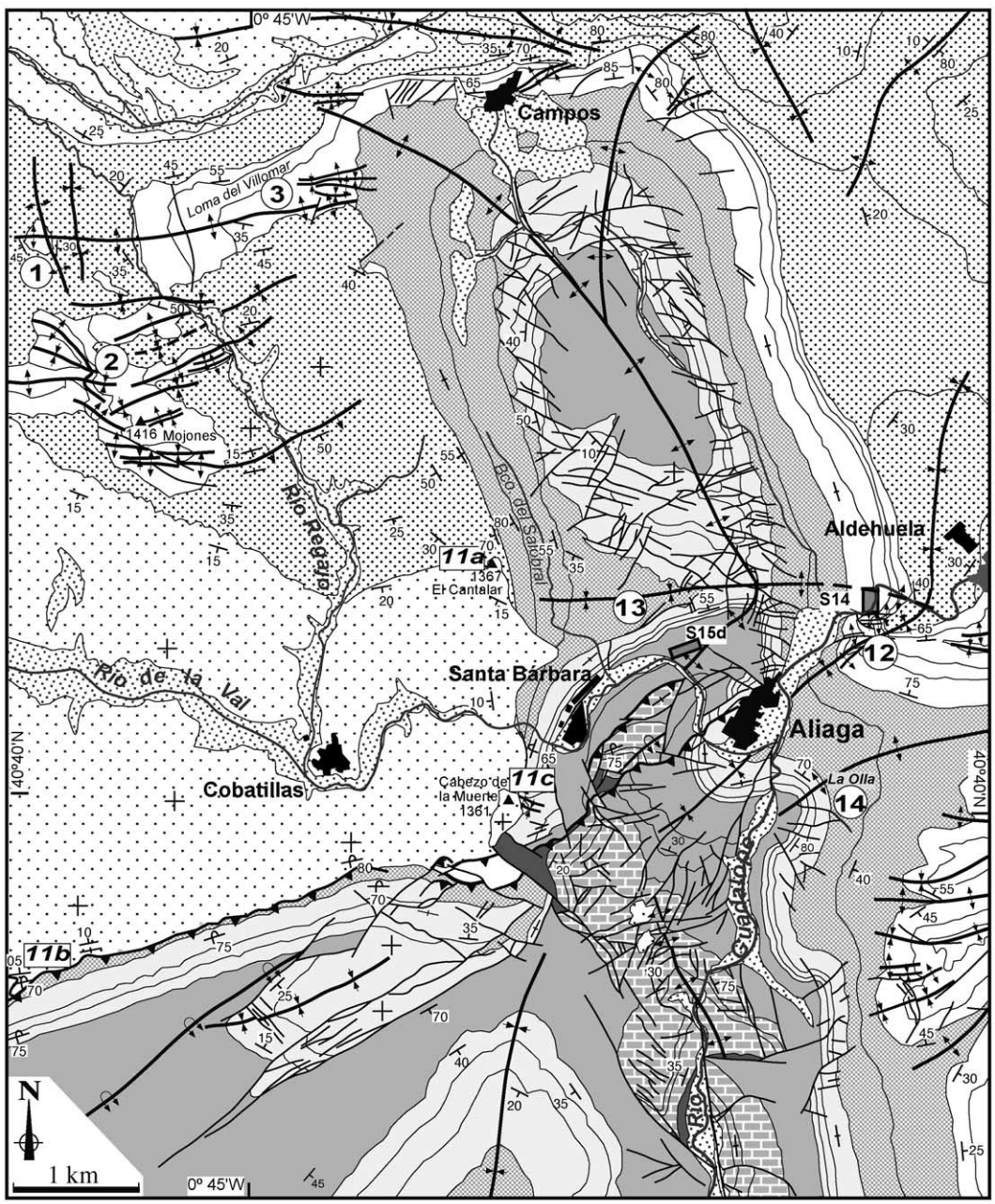
0º 45'W
Campos
Loma del Villomar
3
1
2
1416 Mojones
Río Regajo
Río del Salobral
11a
1367
El Cantalar
Aldehuela
13
S14
S15d
12
Santa Bárbara
Río de la Val
Aliaga
40º40'N
Cobatillas
Cabezo de la Muerte
1361
11c
La Olla
14
11b
Río Guadarrama
N
1 km
0º 45'W

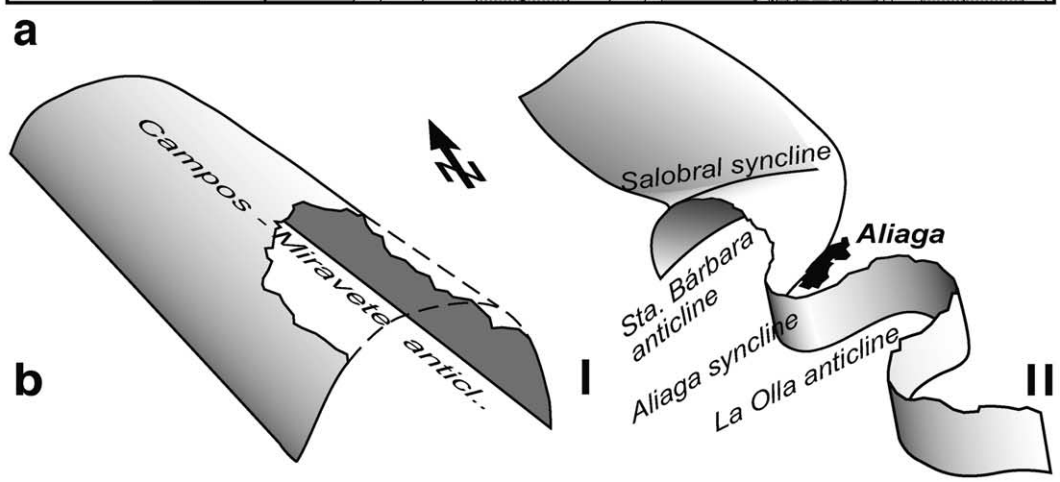
a
b
Campos - Miravete antic.
N
Salobral syncline
Aliaga
Sta. Bárbara anticline
Aliaga syncline
La Olla anticline
I
II

surroundings of Aliaga and give rise to typical structural landforms, such as *La Olla* ('The Pot'; Fig. 8a and b). These folds mainly developed on the eastern limb of the Campos–Miravete anticline, and are strongly disharmonic across the Cretaceous sequence. Some of them involve the competent Urgon facies (mid Lower Cretaceous) and vanish into incompetent materials, which acted as local detachment levels, both below and above the former (Weald facies and Escucha Fm., respectively). Detachment probably impeded refolding of the early axial surface, shortening of the Jurassic core being mainly accommodated by fracturing. Immediately south of Aliaga (site 14 in Figs. 3 and 7a) these structures have kilometric wavelengths, and include the Aliaga syncline, La Olla anticline, as well as two open folds along the eastern margin of the Guadalope river (Fig. 7). Others affect the Upper Cretaceous limestones and dolostones, strongly detached from the Upper Albian sands and Lower Cenomanian marls (site 12 in Figs. 3 and 7a). They exhibit a short (deca- to hectometric) wavelength and, frequently, angular geometry (Fig. 8c and d). Finally, two hectometric snake-like folds involving Urgon units appear on the western limb of the Campos anticline, close to Cabezo de la Muerte (Fig. 11c; site 11c in Fig. 7a).

Snake-like folds constitute a very special type of buckle superposition. They do not have a true geometrical identity (they are simply vertical-axis folds). Also, they could be considered as an extreme case of abutting folds (Type 1d), bearing in mind a theoretical gradual transition between both types as a function of F_1 limb dip. Nevertheless, as we will discuss in Section 7, snake-like folds resulted from mechanical conditions (absence of hinge zone owing to erosion) substantially different from those of abutting folds, so we prefer to assign them to a separate class.

4.3. Standard Type 2

Type 2 fold interferences observed in the Aliaga area all correspond to Type 2a (*Third mode* of Ghosh et al. (1992), see Fig. 4). No Type 2b structure (*Fourth mode*) has been found. The best example is located near La Cañadilla, at the northeastern boundary of the Palaeogene basin (site 7 in Figs. 3 and 9). The axial trace of a large, NW–SE-trending anticline shows sharp undulations produced by superposition of two second-generation, ENE–WSW-trending folds. F_1 and F_2 folds have similar (kilometric) wavelengths. The F_2 folds are conical, with their hinges plunging steeply in opposite directions on both F_1 limbs. Each F_2 anticline on a limb of the F_1 fold continues as a syncline on the other limb. All these features define Type 2a superposition. It is further noteworthy that refolding also involves a NW–SE striking thrust coeval with the F_1 anticline. North of site 7, a third second-generation fold overprints the NW–SE-trending fold where it has lost its northern limb, cut by the thrust. In this case, refolding does not result in a true Type 2a structure because only one F_1 limb is affected.

A similar but smaller-scale example of a Type 2a structure is developed in the Upper Cretaceous limestones of the Mojones anticlinorium (site 2 in Figs. 3 and 7a), where the wavelength of both fold sets (NW–SE-trending F_1, E–W-trending F_2) is only 100–200 m.

The third example is near Aliaga. The E–W-trending Salobral syncline (site 13 in Figs. 3 and 7a) is superposed to the NNW–SSE-trending Campos–Miravete anticline, which shows a strongly curved axial trace north of Aliaga. The Salobral syncline has a pronounced conical shape, widening to the west and narrowing towards the F_1 antiformal hinge (Fig. 7a and b). Sharp bending of the F_1 axial surface gives rise to segmentation of the earlier anticline into two distinctly oriented structures: the NW–SE-trending Campos anticline and the NE–SW-trending Santa Bárbara anticline. The Salobral syncline probably nucleated on an Early Cretaceous fault-related monocline, which could be associated with the Santa Bárbara fault (Soria, 1997) and produced an angular unconformity within the Escucha Fm. (Simón et al., 1999).

A fourth case of Type 2a superposition has been identified north of Montoro de Mezquita, outside the Aliaga area (Fig. 10; see location in Fig. 1) with both fold sets showing kilometre-scale wavelengths. The strongly sinuous Montoro anticline and another parallel F_1 syncline are overprinted by later, NW–SE- to E–W-trending folds. Here, the fold sequence is different from the former examples, and will be discussed in the next section.

5. Evolution and age of folding

The evolution and age of the described superposed folds can be constrained by analysing their relationships with syntectonic Tertiary deposits. Within the Aliaga area, these relationships are clear and agree with interference geometry. NW–SE- to NNW–SSE-trending folds developed during a long period including most of the Eocene and Oligocene times (González and Guimerà, 1993). The eastern limb of the Campos anticline began to form by the mid Eocene (coeval with T2 unit), whereas the development of the western limb finished by the Oligocene–Miocene boundary, giving rise to the angular unconformity between T4 and T5 (Fig. 11a). On the other hand, the ENE–WSW-trending folds probably formed during a shorter period near

Fig. 7. Superposed folds at Aliaga. (a) Geological map; see symbols for stratigraphic units in Fig. 2. Tertiary units mapped according to González (1989). Circled numbers: location of structures described in the text. *11a*, *11b*, *11c*: location of photographs of Fig. 11. S14 and S15d: sites where flexural-slip striations have been measured (see Figs. 14 and 15). (b) 3D sketch of the overall structure for the two successive fold generations (simplified reconstruction for the Urgon limestones, faults not included).

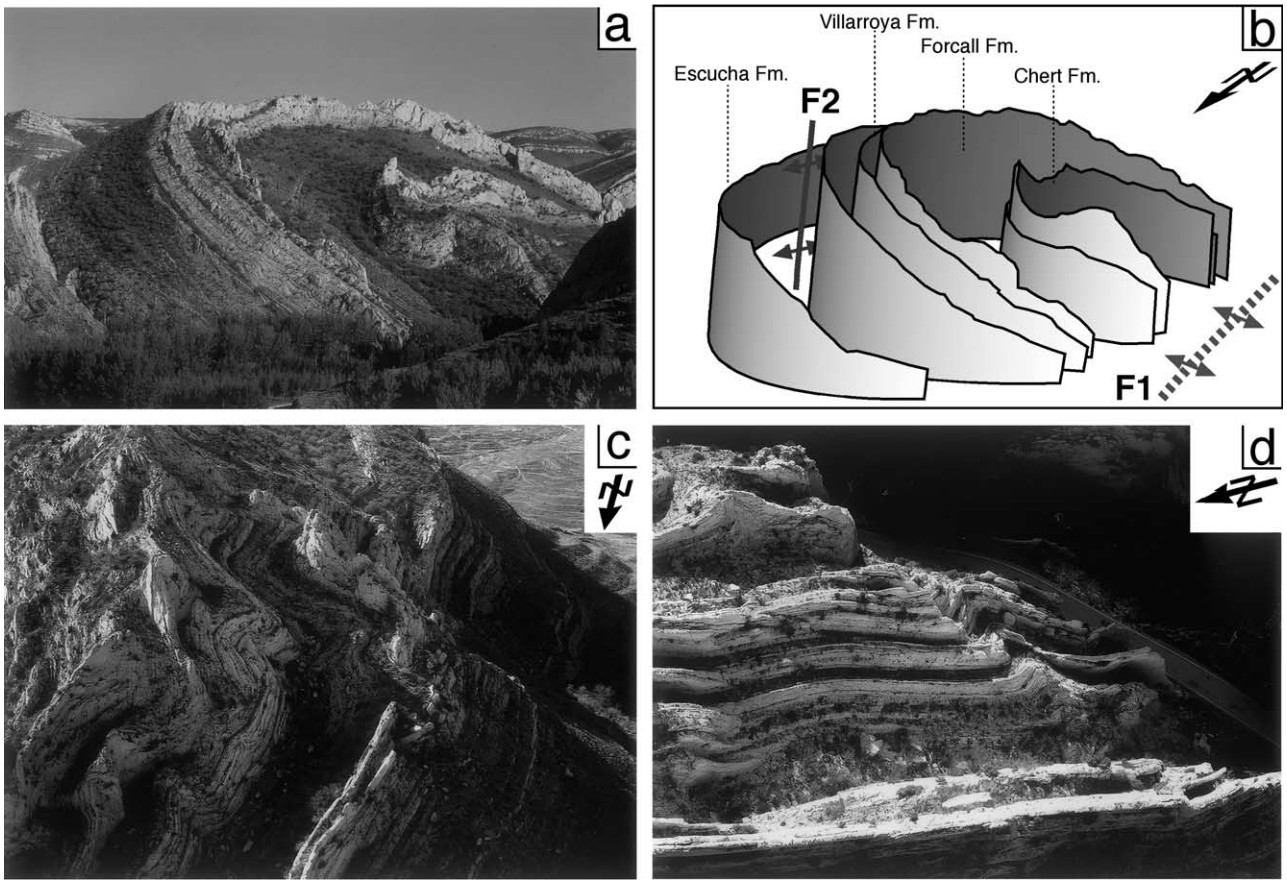

Fig. 8. Field examples of snake-like folds near Aliaga. (a) and (b) Photograph and 3D sketch of *La Olla* ('The Pot') anticline, mainly involving Urgon limestones (site 14 in Fig. 7a). (c) and (d) Low-height aerial photographs of decametric folds in Upper Cretaceous limestones at the Guadalope gorge, between Aliaga and Aldehuela (site 12 in Fig. 7a).

the T5–T6 limit (Early Miocene; Simón et al., 1998). T5 conglomerates are affected by ENE folds and thrusts in the Cobatillas area (Fig. 11b), whereas flat-lying T6 conglomerates of the Cabezo de la Muerte lie unconformably on Urgon limestones affected by ENE-trending, vertical-axis folds (Fig. 11c).

Tectonosedimentary relationships from other areas east of Aliaga suggest that individual folds showing similar trends can be strongly diachronous throughout the region (Fig. 12). The ENE–WSW-trending fold at Los Olmos (Fig. 6), while overprinting a NW–SE-trending anticline as well, is older than those of Aliaga. The first-generation fold deforms T1 and T2 units and predates T3, while the second-generation, ENE-trending structure postdates T3 (González, 1989). Near Berge, east of Los Olmos (Fig. 6), ENE-trending folds even had initiated prior to T3. The strongly sinuous axial trace of the Montoro anticline (Fig. 10) would represent the modified hinge of a NE–SW-trending anticline overprinted by younger NW–SE- and E–W-trending folds, and cut by the N–S structures at the eastern boundary of the Aliaga Tertiary basin. Since the latter are probably coeval with T4 (González and Guimerà, 1993), the NE–SW-trending anticline of Montoro probably predates T4. Finally, NE–SW-trending folds at Las Cuevas de Cañart (15 km northeast of Montoro de Mezquita; see location in Fig. 1) also predate T4 deposits and are overprinted by E–W-trending folds deforming T4 and T5 (González et al., 1985).

These relationships indicate that the large NE–SW compressional structures east of the Montalbán thrust (Fig. 1) are older than the ENE–WSW-trending folds of Aliaga, and partially coeval with NW–SE folds in the overall region (Guimerà, 1988; González, 1989). Fig. 12 sketches the space/time distribution of the three fold sets so defined.

Palaeogene deposits at the eastern sector of the Aliaga Tertiary basin show a number of L- and T-shaped buckle interferences composing a complex structural pattern that requires further analysis. Some of them give rise to triple junctions of syncline traces (sites 4, 5, 9 and 10 in Fig. 3) where time relationships between different fold directions are difficult to establish. Guimerà (1988) interpreted this fold ensemble as a result of monophase constrictional deformation. Nevertheless, according to the experimental models by Skjernaa (1975), Ghosh et al. (1993) and Johns and Mosher (1996), these L- and T-shaped patterns could also form by superposition of successive fold sets.

Diagnostic features of coeval, non-coaxial buckle folding include (Ghosh and Ramberg, 1968; De Beer, 1995; Ghosh

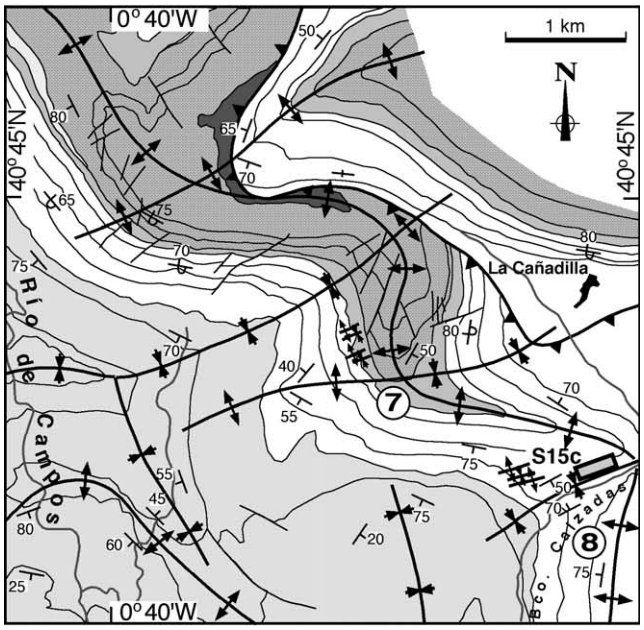

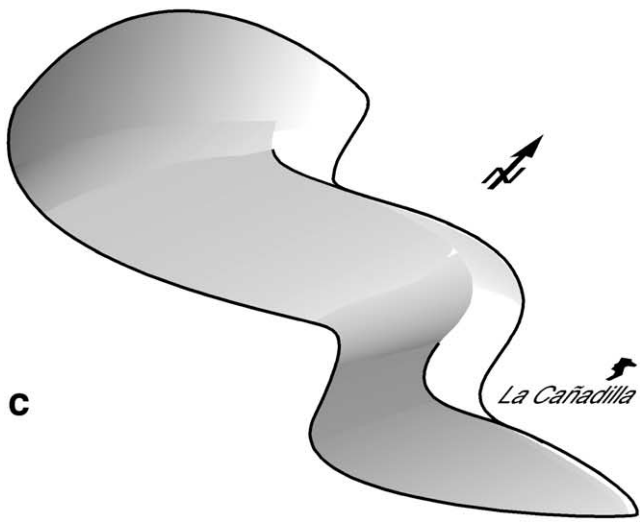

Fig. 9. Superposed folds at La Cañadilla (Type 2a). (a) Geological map; see symbols for stratigraphic units in Fig. 2. Partially based on Canérot et al. (1979). Tertiary units mapped according to González (1989). S15c: site where flexural-slip striations have been measured (see Fig. 15b and c). (b) Aerial photograph of the central part of the mapped zone. (c) 3D sketch of the overall structure (simplified reconstruction for the Lower–Upper Cretaceous boundary, thrust not included).

et al., 1995): (a) irregular curving fold trends and non-cylindrical shapes; (b) non-plane non-cylindrical folds closely associated with domes and basins, (c) fold hinge bifurcations, (d) highly variable fold trends, and (e) inconsistent age relationships between different fold trends. Features (a)–(c) are inconclusive since they could also develop during Type 2 or modified Type 1 superposition. The distribution of fold trend frequencies (Fig. 13) shows two clear maxima, NNW–SSE and ENE–WSW, which works against criterion (d). Criterion (e) cannot be applied in this case because no fold axial trace overprints another. So, no conclusive geometrical argument supports the hypothesis of coeval folding.

Unfortunately, tectonosedimentary timing evidence is unclear in this sector of the Tertiary basin. Nevertheless, it may be significant that ENE–WSW-trending folds involve the complete Palaeogene series (T1–T4), whereas NW–SE-trending folds vanish into T3 (site 10 in Fig. 3) or are associated with unconformities between T3 and T4 (sites 4 and 9).

In summary, we cannot exclude the possibility of the occurrence of local domains where both fold sets were partially coeval (constrictional deformation), but triple junctions can also represent T-shaped patterns formed by juxtaposition of two essentially non-coeval folds. According to the general sequence inferred at Aliaga, cases marked as 5 and 10 could be classified as joined folds (Type 1c), and cases 4 and 9 as abutting folds (Type 1d).

6. Microstructural data: details about kinematics of fold superposition and hinge replacement

Small-scale structures related to both folding episodes (stylolites, faults, flexural-slip striations) are abundant in the study area. They were mainly observed in the Upper Cretaceous limestones at the eastern, near-vertical limb of the Campos anticline, subsequently affected by snake-like folds of deca- to hectometric wavelength. Here, two sets of flexural-slip striations were observed: (a) earlier ‘dip-slip’ striations (FS1) related to the Campos anticline, (b) later ‘strike-slip’ striations (FS2) related to vertical-axis folds (Fig. 14a). These data confirm the occurrence of two separate folding events and their relative timing. Such striations were systematically measured on nearly vertical bedding surfaces along the road between Aliaga and Aldehuela (site S14 in Fig. 7a). Second-generation striations are more abundant. Their distribution fits a near vertical,

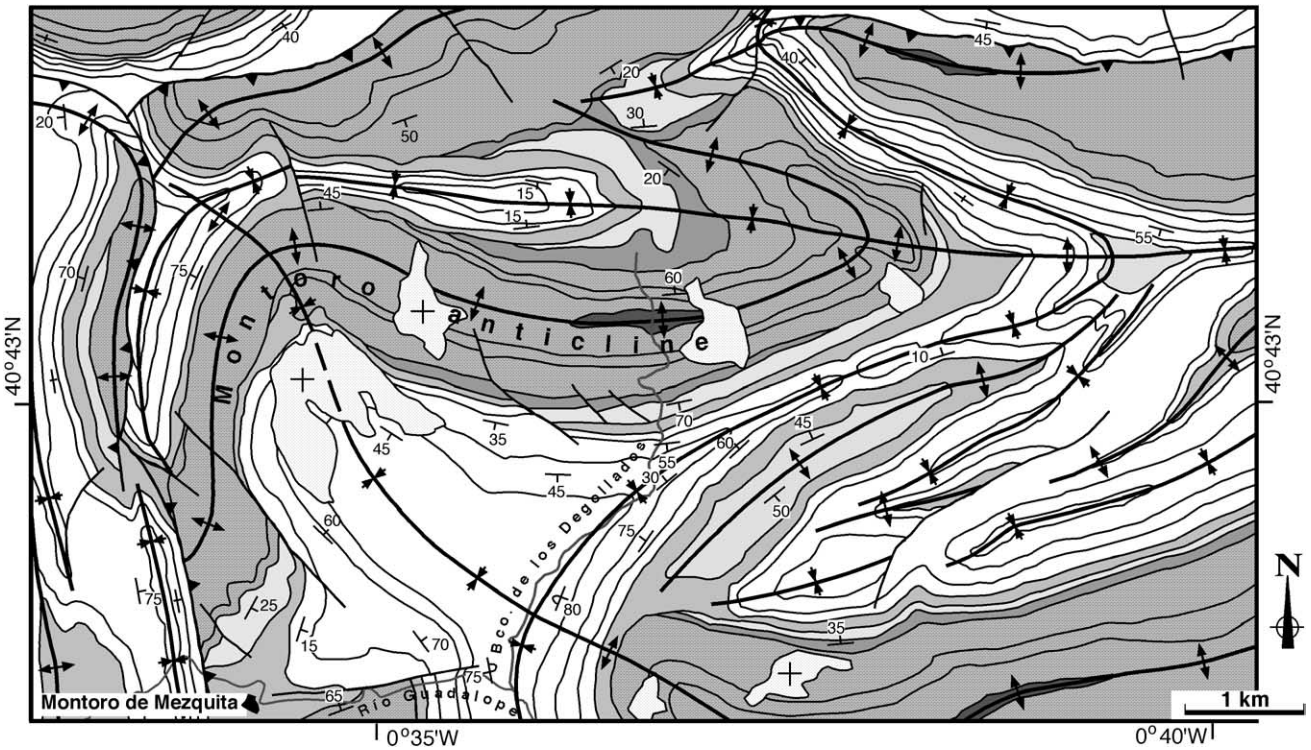

Fig. 10. Superposed folds at Montoro de Mezquita (Type 2a). See symbols for stratigraphic units in Fig. 2. Modified from Canérot et al. (1979).

slightly conical F_2 fold, showing movement senses consistent with their location on both fold limbs: left-lateral movement on the southern, NE–SW striking limb; right-lateral movement on the northern, N–S striking limb (Fig. 14b and c).

In cases of Type 2 superposition, progressive change in both location and orientation of the hinge line makes it difficult to distinguish between both generations of flexural-slip striations. 'Hinge migration' (Odonne, 1987; Odonne and Vialon, 1987) or 'hinge replacement' (Ghosh et al., 1992, 1996) is a mechanism concomitant with Type 2 buckle superposition, which results from kinematic problems during simultaneous rotation of opposite F1 fold limbs about two differently oriented F_2 axes. A sinuous hinge is newly created as the old F_1 hinge unfolds and disappears (Fig. 15a). Although it resembles a strongly curved F_1 hinge, it is in reality a new line (F'_1) developed under the second deformation. F'_1 moves into the convex side of the superposed fold while the line parallel to F_1 moves into the concave side. So, the latter is less curved than F'_1 and transects the sinuous new hinge (Ghosh et al., 1992; Grujic, 1993). Since the hinge line does not behave as a passive line during refolding, F'_1 cannot be 'unrolled' in order to reconstruct its original trace. As an example, if we tried to unroll passively the sinuous axial trace of the Montoro anticline (Fig. 10) we would find unsolvable space problems.

Bed surfaces observed within two representative examples of Type 2 superposition (La Cañadilla, site S15c in Fig. 9a; Aliaga, site S15d in Fig. 7a) show varied flexural-slip striations, which could be related to such changes in position and orientation of fold hinges. Dispersion of striation rakes on bedding planes is very high in both cases (Fig. 15c and d). They are tentatively attributed to each folding stage by (a) calculating the most probable orientation of each fold axis (F_1, F'_1 and F_2), and (b) selecting striation sets that are oriented at right angles to those axes and show slip sense (inferred either from crystal fibres or small slickolites) compatible with flexural-slip conditions. As an example, Fig. 15b sketches the model of theoretical relationships between fold axes and flexural-slip striations at La Cañadilla, which allows the explanation of the collected data.

7. Discussion: conditions for development of each type of superposed buckling

The primary condition that Types 1 and 2 of superposed folds require is a small angle between the trend of the earlier folds and the later direction of shortening (Ghosh and Ramberg, 1968). This condition is fulfilled in the studied region, since both directions are near parallel in most cases.

On the other hand, a number of geometrical parameters of the first-generation folds (tightness, curvature and fold wavelength) have been invoked as factors controlling the occurrence of either Type 1 or Type 2 geometry (Ghosh and Ramberg, 1968; Skjernaa, 1975; Watkinson, 1981; Odonne and Vialon, 1987; Ghosh et al., 1992; Grujic, 1993). Type 1 tends to develop if first-generation folds are gentle, rounded

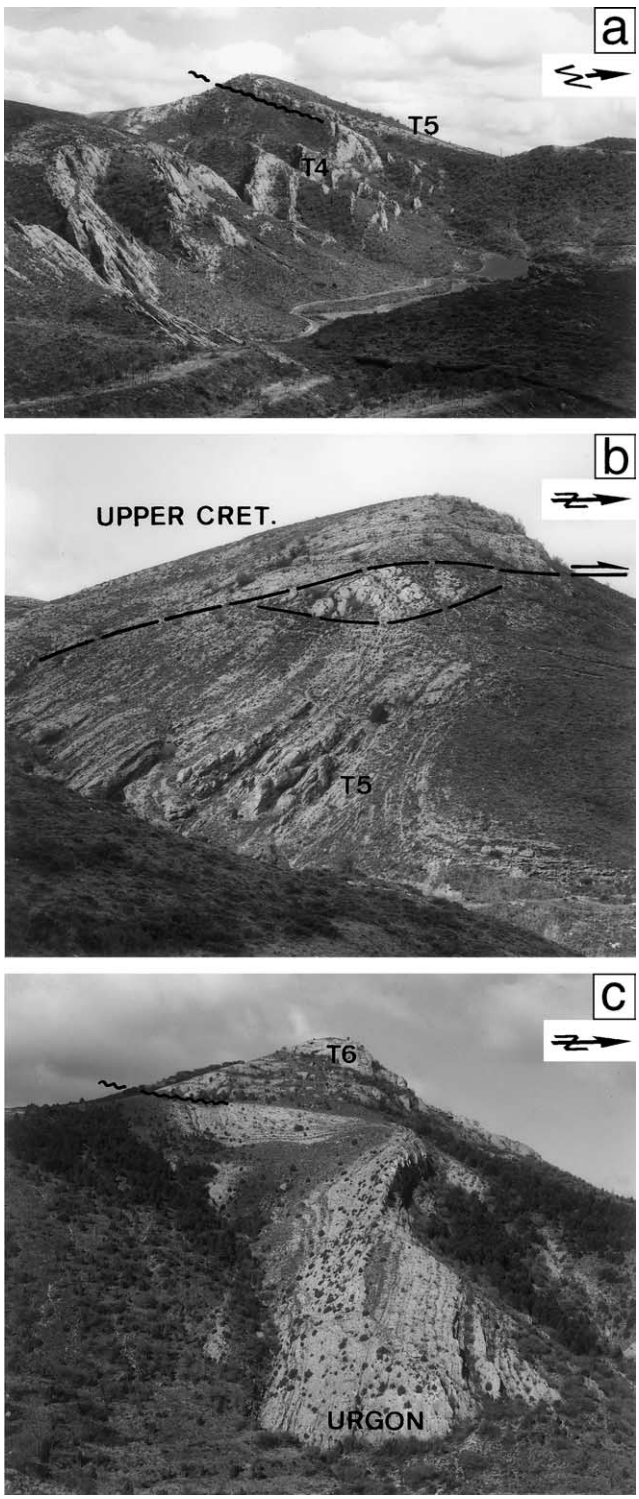

Fig. 11. Field relationships between superposed folds and Tertiary deposits surrounding Cobatillas; see location in Fig. 7a. (a) Angular unconformity between vertical beds of T4 (Late Oligocene) and gently dipping beds of T5 (Oligocene–Miocene transition) at El Cantalar; this unconformity allows the dating of the western limb of the Campos anticline. (b) T5 conglomerate beds bended within the footwall of the ENE-striking Cobatillas thrust. (c) Angular unconformity between Urgon limestones, affected by snake-like folds, and flat-lying conglomerates of Cabezo de la Muerte (T6, middle Miocene).

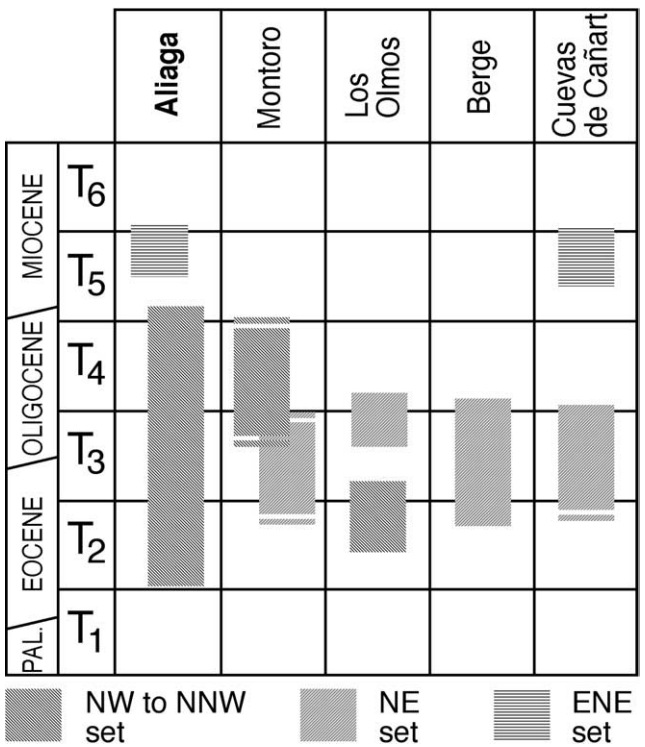

Fig. 12. Approximate chronology of interfering fold sets in the northeastern Iberian Chain, according to the observed tectonosedimentary relationships. T1–T6: tectonosedimentary units defined by González (1989).

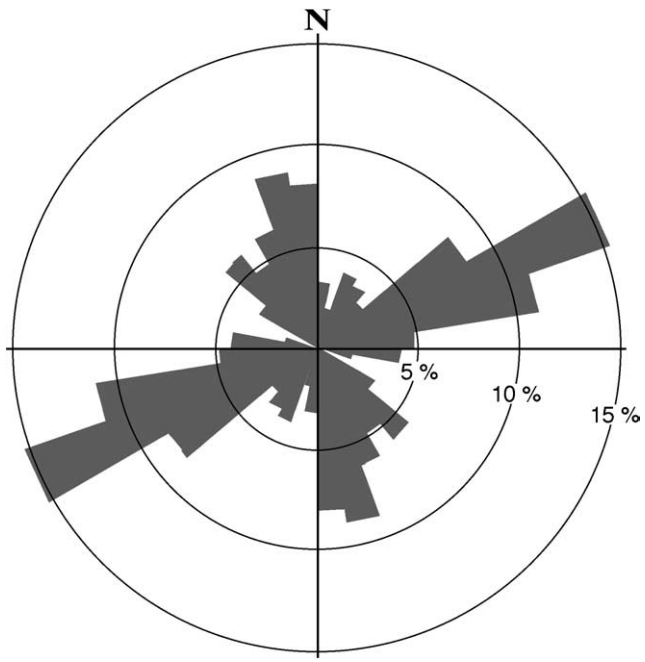

Fig. 13. Rose diagram of fold trend frequency in the Palaeogene deposits east of Aliaga.

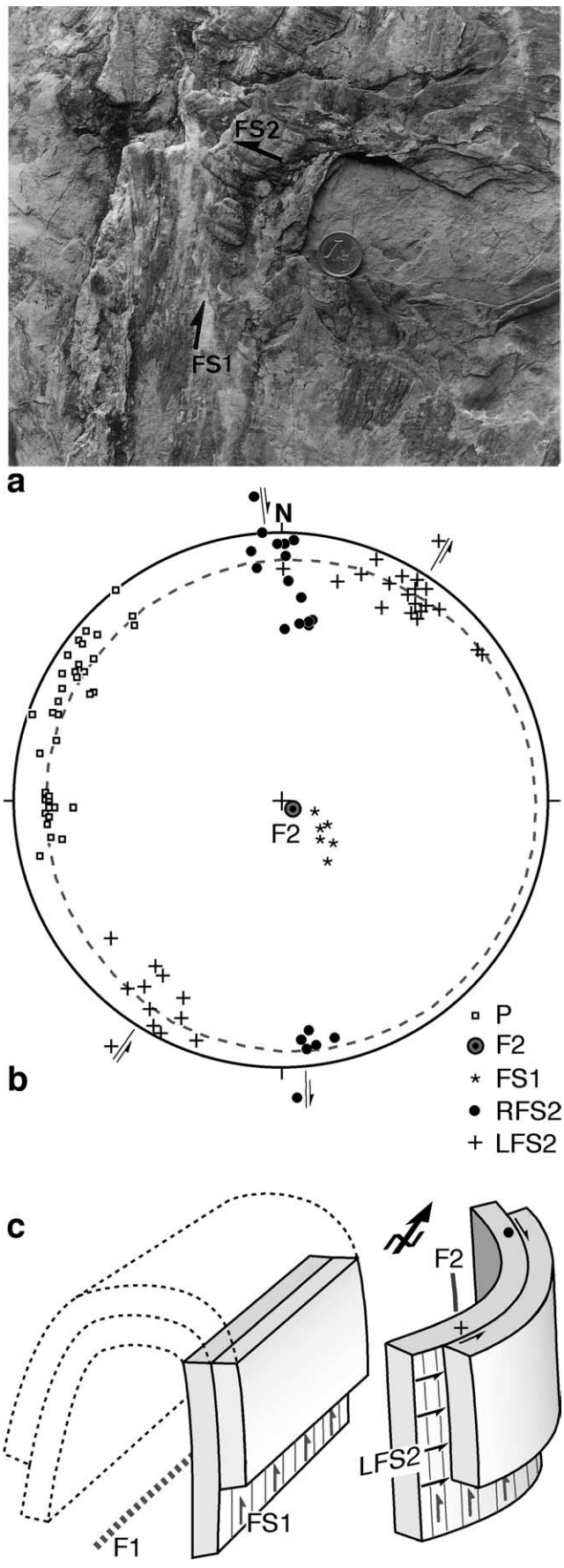

Fig. 14. (a) Flexural 'strike-slip' striations related to snake-like folds (FS_2) overprinting 'dip-slip' striations on the eastern limb of the Campos anticline (FS_1). (b) Equal-area plot of measured and inferred structural elements. (c) 3D sketch explaining the superposition of flexural-slip striations. P: poles of bed planes; F_1 and F_2: axes of first- and second-generation folds, respectively; FS_1: flexural-slip striations related to F_1; RFS_2 and LFS_2: right-lateral and left-lateral striations, respectively, related to F_2. See location of measurements in Fig. 7a, site S14.

and relatively wide, whereas high tightness, high curvature and long amplitude favour development of Type 2. Among the former parameters, hinge curvature and fold amplitude could not be measured in our field examples owing to the severe erosion of most earlier hinge zones. The other parameters (interlimb angle and relative fold wavelength) were analysed, the results showing good agreement with those arising from published analogue models (see Table 1 and Fig. 16). The case studied at Los Olmos has not been included owing to its large dimensions (7×15 km) and isolated location.

Many researchers (Odonne and Vialon, 1987; Ghosh et al., 1992; Grujic, 1993) state that the interlimb angle of the earlier folds constitutes the primary control on interference geometry. According to the experimental models, early folds showing interlimb angles exceeding 70–90° refold into Type 1 geometry, whereas those with smaller interlimb angles refold into Type 2 (Table 1 and Fig. 16). Ghosh et al. (1992) point out that these boundary values may only serve for particular experimental conditions and they may change as the viscosity ratio varies. Nevertheless, the kinematic analysis by Grujic (1993) suggests that 90° is actually a critical value for the F_1 interlimb angle, at which the probability of being refolded into either Type 1 or Type 2 geometry is the same. In our field cases, values of interlimb angle ranging approximately from 85 to 95° apparently limit the development of Type 1 and Type 2 (see Table 1 and Fig. 16). So, the influence of tightness of the earlier folds on the type of buckle superposition, upheld by all the mentioned authors, appears to be corroborated by field examples in the Aliaga region. Moreover, the critical interlimb angle close to 90° observed in real folds (with scale and rheology quite different from those of analogue models) fits Grujic's analysis.

The relative wavelength of F_1 and F_2 folds (W_1/W_2) is itself a result of the particular conditions in which refolding occurred, showing varied relationships with interference types (Fig. 16). For Types 1a and 1b, this relationship is inherent in their definition: Type 1b interferences necessarily form with $W_1 > W_2$, whereas structures showing $W_1 \leq W_2$ will be classified as Type 1a. Also, Types 1c and 1d develop with different wavelength ratios: $W_1 > W_2$ for Type 1d and $W_1 \leq W_2$ for Type 1c. This suggests that, in the case of abutting folds (Type 1d), W_2 is reduced with respect to that developed in the corresponding flat layers (W_1), owing to mechanical constraints similar to those demonstrated by Ghosh (1970) for Type 1b. On the

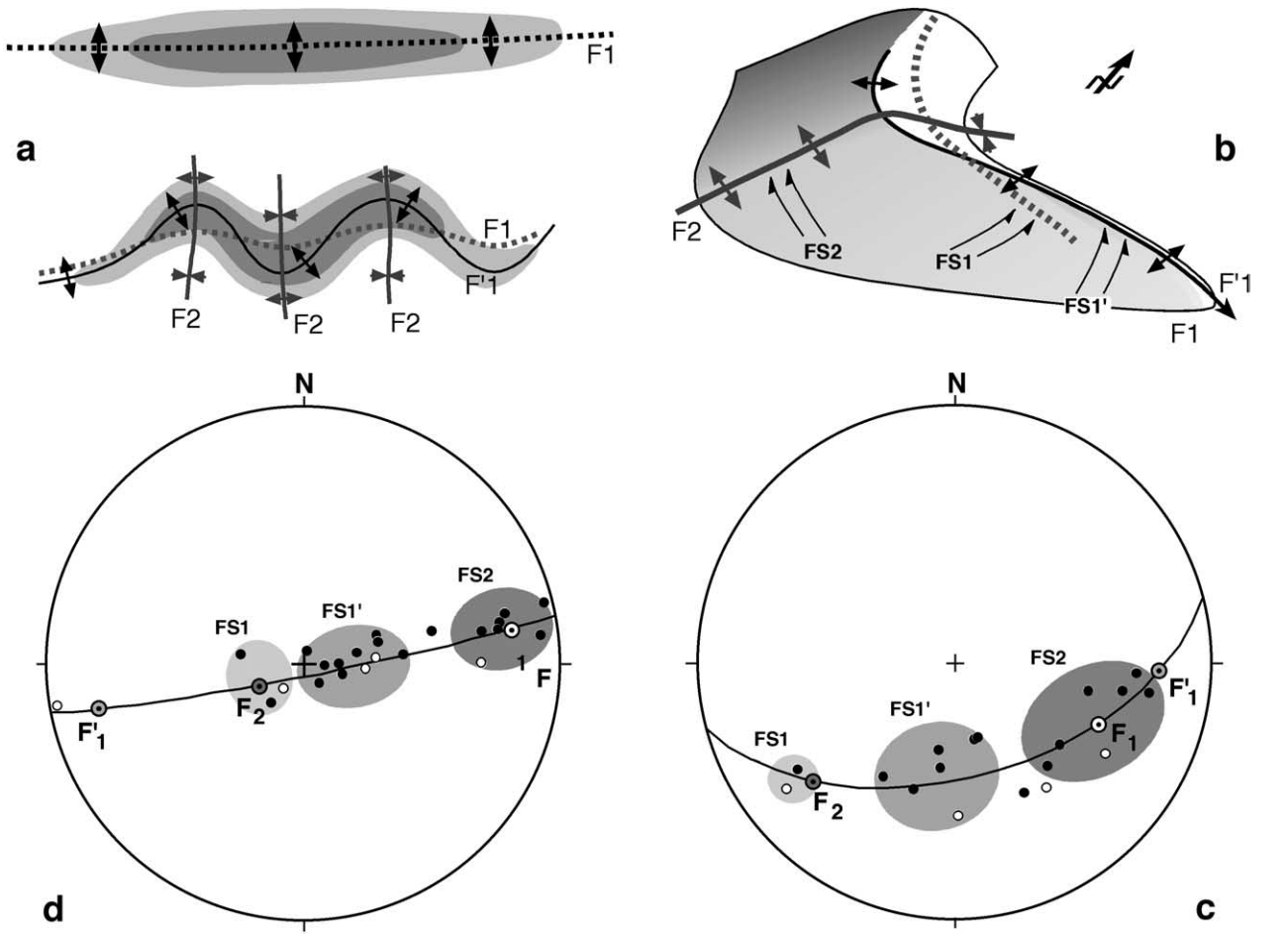

Fig. 15. Evidence of hinge replacement in Type 2 superpositions. (a) The concept of hinge replacement according to Ghosh et al. (1992, 1996); F_1: material line parallel to the true first-generation hinge line; F'_1: apparent, modified first-generation hinge line; F_2: second-generation hinge line. (b) Sketch of a portion of La Cañadilla structure showing tentative orientation of F_1, F'_1 and F_2, as well as the corresponding sets of flexural-slip striations (FS_1, FS'_1 and FS_2, respectively) on its southernmost limb. (c) Equal-area plot of measured flexural-slip striations (average orientation of bedding represented by the great circle); a group of striations has been interpreted to be related to each hinge line (F_1, F'_1 and F_2) at right angles to it; black dots: striations showing sense of movement compatible with flexural slip; white dots: striations with unknown sense of movement. (d) Idem on the northern limb of Santa Bárbara anticline. See location of both sites in Fig. 9a (S15c) and Fig. 7a (S15d).

Table 1
Comparison between interlimb angles of earlier folds described in analogue models of each type of buckle superposition and those measured in the studied field cases

		Interlimb angle of earlier folds (°)			
		Aliaga folds	Analogue models		
			Ghosh et al. (1992)	Grujic (1993)	Odonne and Vialon (1987)
Type 1	1a	105	>135	>90	>70
	1b	90–95	90–135		
	1c	85–128			
	1d	90–115			
	1e	75			
Type 2	2a	40–95	30–95	>90	>70
	2b		<30	<90	<70

contrary, joined folds (Type 1c) would initiate independently in the presence of F_1 and develop wavelengths close to W_1. Finally, Type 2 structures show no distinct wavelength ratio with respect to Type 1.

Lateral terminations of first-generation folds are zones where later near-orthogonal folds can be easily joined, owing to the favourable orientation of beds (strike at right angles to the fold trend). This occurs at the northern extremity of the Campos anticline (Figs. 3 and 7a), where second-generation, E–W-trending folds were joined. In the same way, culminations and depressions of first-generation hinges may help second-generation folds to ride over the former, giving rise to Type 1 superposition in conditions where this would not be allowed. This is the case in the Barranco de las Calzadas syncline (site 8 in Figs. 3 and 9a), where an upright isoclinal fold developed on an antiformal depression in La Cañadilla anticline. While refolding of the latter is mainly a Type 2 superposition, a Type 1b syncline developed across the early antiform at this site.

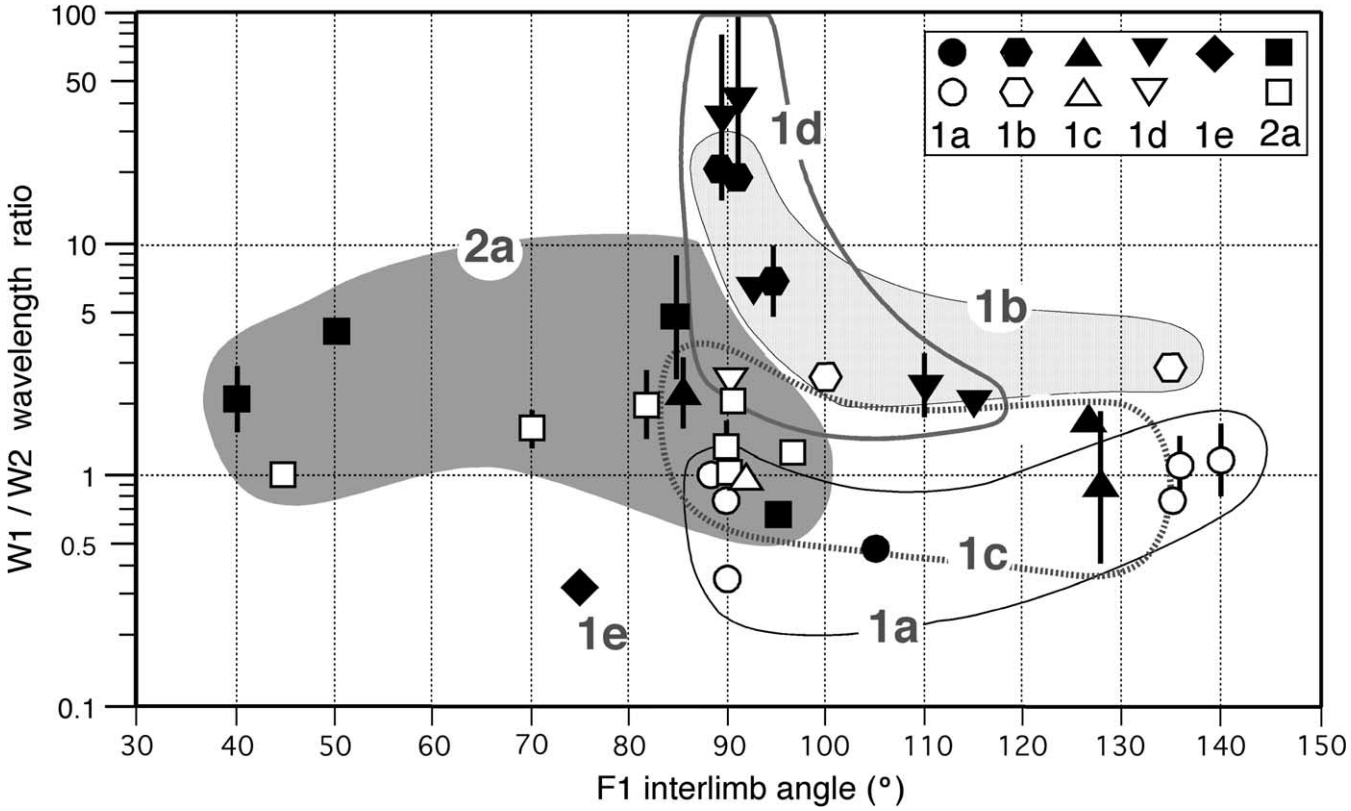

Fig. 16. Values of interlimb angle of earlier folds (F_1) versus wavelength ratio (W_1/W_2) in different types of natural and experimental superposed folds. Black symbols: natural examples in the Aliaga area. White symbols: experimental models by Ghosh et al. (1992) and Grujic (1993); in these cases, values of the plotted parameters have been either taken from the descriptions made by the authors or estimated from their published photographs.

In addition, the mechanical behaviour of layered rocks controls the interference geometry. According to Lisle et al. (1990), Type 1 interference is incompatible with isometric folding. So, conditions affecting strain partitioning between layer-parallel shortening and buckling will have an influence on the superposition type (Johns and Mosher, 1996). High ductility and low viscosity ratio between competent and incompetent layers give rise to high layer-parallel shortening, which allows development of non-isometric folding and so Type 1 superposition. On the contrary, low ductility and high competence contrast favours Type 2 superposition. Tertiary folds described in Aliaga developed at near-surface conditions, as indicated by their relationships with syntectonic alluvial deposits. On the other hand, they deformed competent carbonate units alternating with soft sandstones and lutites (Fig. 2). So, the folded materials would have shown both a low average ductility and a high viscosity ratio, which probably inhibited the formation of dome-and-basin structures, while favouring Type 2 and modified Type 1 superposition.

The genetic conditions of snake-like folds merit specific discussion. These structures resulted from longitudinal shortening of the near vertical limbs of the previous box-shaped, NNW–SSE-trending Campos–Miravete anticline, also favoured by viscosity contrast. They have the same origin as the Type 2 structure found immediately north of Aliaga (Salobral syncline). Why do we observe these quite different geometries? In our opinion, the development of vertical-axis folds (especially those large ones affecting the Urgon units) essentially represents single buckling of vertical layers. For this process to occur, mechanical resistance from the previous fold hinge should have been removed in the competent Urgon limestones (on the contrary, a Type 2 structure probably would have formed). That condition might have been accomplished by previous erosion of the anticline hinge (the syncline hinge being deep or rounded enough). At present, erosion has not completely broken the continuity of the Urgon units across the hinge zone north of Aliaga, whereas the Urgon crest has completely disappeared from the southern sector (see Fig. 7a). The Jurassic core already cropped out when refolding occurred, as indicated by Jurassic limestone pebbles within the syntectonic T5 alluvial fill of the Cobatillas basin. Thus, we believe that, south of Aliaga, the previous hinge zone in the Urgon facies had been eroded away before the vertical folds developed, while this hinge zone was preserved north of Aliaga favouring Type 2 superposition.

In this way, snake-like folds illustrate the interdependence between internal and external processes during mountain building (Dahlen and Suppe, 1988).

8. Summary and conclusions

The Aliaga area shows spectacular examples of large-scale buckle superposition analogous to those described in experimental models. They developed by interference between earlier NNW–SSE-trending folds (Eocene–Oligocene in age) and later ENE–WSW-trending ones (Early Miocene). Their direction and ages are compatible with intraplate Alpine compression normal (NE) and longitudinal (SE–SSE), respectively, to the Iberian Chain (*Iberian* and *Betic* stress fields as defined by Liesa (2000)). To the east, the conspicuous ENE–WSW- to NE–SW-trending folds and thrusts in the Montoro–Alcorisa area make up a third set, older than the ENE–WSW set at Aliaga and partially coeval with NW–SE folds in the overall region. They were probably induced by left-lateral reactivation of a late-Variscan, NE–SW striking wrench fault (Simón, 1984), their direction not being directly related to far-field compression.

The superposed folds have been classified following the criteria proposed by Thiessen and Means (1980), Ghosh and Ramberg (1968), Skjernaa (1975) and Ghosh et al. (1992), although using a slightly modified nomenclature (see Fig. 4):

- Standard Type 1: (1a) dome-and-basin structure, (1b) unequal-wavelength overprinted folds.
- Modified Type 1: (1c) T-shaped 'joined' folds, (1d) T-shaped 'abutting' folds, (1e) L-shaped folds, (1f) 'snake-like' folds.
- Standard Type 2: (2a) non-cylindrical buckling of earlier axial surfaces involving hinge replacement.

Successive sets of flexural-slip striations measured at Aliaga–Aldehuela and La Cañadila help us to analyse kinematics of fold superposition. Near-horizontal striations related to snake-like folds at Aldehuela overprint near-vertical striations related to the earlier NNW–SSE-trending Campos anticline. In cases of Type 2 interference (La Cañadilla, Aliaga), flexural-slip striations could develop associated with both the earlier fold hinge (F_1) and the new one resulting from hinge replacement (F'_1), apart from those related to the second-generation fold (F_2). This confirms that F_1 hinge lines do not deform as passive markers; on the contrary, they maintain their role as active folding axes while they change into F'_1 hinges.

Fold interference geometry is mainly controlled by the interlimb angle of first-generation folds. In the studied cases, Types 1 and 2 typically appear for F_1 interlimb angles over and below 90°, respectively, which is consistent with the kinematic analysis by Grujic (1993). On the other hand, the relative wavelength of F_1 and F_2 varies for different subtypes within Type 1. Type 1a shows $W_1/W_2 \leq 1$, whereas Type 1b shows $W_1/W_2 > 1$, which is inherent in their definition. Type 1c occurs with lower W_1/W_2 ratios than Type 1d, which suggests that abutting folds (1d) undergo mechanical constraints analogue to those of Type 1b, whereas joined folds (1c) can develop with independent wavelengths close to W_1. This argument could provide a key to distinguish joined from abutting folds, and so approach fold timing in T-shaped patterns based on geometrical criteria.

Other secondary factors can also influence the geometry of buckle superposition. Lateral terminations and antiformal depressions of first-generation folds are zones where later near-orthogonal folds may be easily formed, owing to the favourable orientation of beds. Rheology affects strain partitioning between layer-parallel shortening and buckling. Specifically, high viscosity contrast between adjacent beds inhibits layer-parallel shortening and non-isometric folding, favouring Type 2 against Type 1 superposition. Finally, since folding occurred near the surface, erosion processes can also play a key role. We interpret that snake-like folds developed when the pre-existing hinge zone of the Aliaga–Miravete anticline was eroded away. Removal of the main mechanical obstacle for refolding enabled the eastern limb to refold independently into vertical-axis, snake-like folds.

Acknowledgements

I thank Profs. S.K. Ghosh, K.M. Johnson, D. Aerden and another anonymous referee for their interesting comments and criticisms, which were particularly determinant for designing the proposed classification of superposed folds. I also thank Drs L.E. Arlegui and A. González, who read the first version of the manuscript, and especially Dr R.J. Lisle, who kindly and carefully made a final review of the paper. Dr A.M. Casas provided the original draw for the cross-section of Fig. 1b. Photographs 8b and c where made by MRW-Zeppeline. The research was supported by project BTE 2002-04168 of D.G.E.S. (Ministerio de Ciencia y Tecnología, Spanish Government).

References

Aller, J., Gallastegui, J., 1995. Analysis of kilometric-scale superposed folding in the Central Coal Basin (Cantabrian zone, NW Spain). Journal of Structural Geology 17, 961–969.

Alvarez-Marrón, J., 1995. Three-dimensional geometry and interference of fault-bend folds: examples from the Ponga Unit, Variscan belt, NW Spain. Journal of Structural Geology 17, 549–560.

Canérot, J., Crespo, A., Navarro, D., 1979. Mapa Geológico de España, 518 (Montalbán). IGME, Madrid, scale 1:50,000.

Capote, R., Muñoz, J.A., Simón, J.L., Liesa, C.L., Arlegui, L.E., 2002. Alpine tectonics I: the Alpine system north of the betic cordillera. In: Gibbons, W., Moreno, T. (Eds.), Geology of Spain, Geological Society of London, London.

Casas, A.M., Casas, A., Pérez, A., Tena, S., Barrief, L., Gapais, D., Nalpas, T., 2000. Syn-tectonic sedimentation and thrust-and-fold kinematics at the intra-mountain Montalbán Basin (northern Iberian Chain, Spain). Geodinamica Acta 1, 1–17.

Dahlen, F.A., Suppe, J., 1988. Mechanics, growth, and erosion of mountain

belts. In: Clark, S.P., Burchfield, B.C., Suppe, J. (Eds.), Processes in Continental Lithospheric Deformation. Geological Society of America Special Paper 218, pp. 161–178.

De Beer, C.H., 1995. Fold interference from simultaneous shortening in different directions: the Cape Fold Belt syntaxis. Journal of African Earth Sciences 21, 157–169.

Ghosh, S.K., 1970. A theoretical study of intersecting fold patterns. Tectonophysics 9, 559–569.

Ghosh, S.K., 1993. Structural Geology: Fundamentals and Modern Developments. Pergamon Press, Oxford.

Ghosh, S.K., Ramberg, H., 1968. Buckling experiments on intersecting fold patterns. Tectonophysics 5, 89–105.

Ghosh, S.K., Mandal, N., Khan, D., Deb, S.K., 1992. Modes of superposed buckling in single layers controlled by initial tightness of early folds. Journal of Structural Geology 14, 381–394.

Ghosh, S.K., Mandal, N., Sengupta, S., Deb, S.K., Khan, D., 1993. Superposed buckling in multilayers. Journal of Structural Geology 15, 95–111.

Ghosh, S.K., Khan, D., Sengupta, S., 1995. Interfering folds in constrictional deformation. Journal of Structural Geology 17, 1361–1373.

Ghosh, S.K., Deb, S.K., Sengupta, S., 1996. Hinge migration and hinge replacement. Tectonophysics 263, 319–337.

González, A., 1989. Análisis tectosedimentario del Terciario del borde SE de la Depresión del Ebro (sector bajoaragonés) y de las cubetas ibéricas marginales. Ph.D. thesis, Universidad de Zaragoza.

González, A., Guimerà, J., 1993. Sedimentación sintectónica en una cuenca transportada sobre una lámina de cabalgamiento: la cubeta terciaria de Aliaga. Revista de la Sociedad Geológica de España 6, 151–165.

González, A., Pardo, G., Villena, J., Martínez, B., 1985. Análisis tectosedimentario del Terciario de Cuevas de Cañart (prov. Teruel). Trabajos de Geología 15, 169–176.

Grujic, D., 1993. The influence of initial fold geometry on Type 1 and Type 2 interference patterns: an experimental approach. Journal of Structural Geology 15, 293–307.

Guimerà, J., 1988. Estudi estructural de l'enllaç entre la Serralada Ibérica y la Serralada Costanera Catalana. Unpublished Ph.D. thesis, Universidad de Barcelona.

Guimerà, J., Salas, R., 1996. Inversión terciaria de la falla normal mesozoica que limitaba la subcuenca de Galve. Geogaceta 20, 1701–1703.

Johns, M.K., Mosher, S., 1996. Physical models of regional fold superposition: the role of competence contrast. Journal of Structural Geology 18, 475–492.

Julivert, M., Marcos, A., 1973. Superposed folding under flexural conditions in the Cantabrian zone (Hercynian cordillera, northwestern Spain). American Journal of Science 273, 353–375.

Liesa, C., 2000. Fracturación y campos de esfuerzos compresivos alpinos en la Cordillera Ibérica y el NE peninsular. Ph.D. thesis, Universidad de Zaragoza.

Lisle, R.J., 1988. Geological Structures and Maps. A Practical Guide. Pergamon Press, Oxford.

Lisle, R.J., 1992. Constant bed-length folding: three-dimensional geometrical implications. Journal of Structural Geology 14, 245–252.

Lisle, R.J., Styles, P.S., Freeth, J., 1990. Fold interference structures: the influence of layer competence contrast. Tectonophysics 172, 197–200.

Marin, Ph., Pallard, B., Duval, B., Miroschedji, A., 1977. Mapa Geológico de España, 494 (Calanda). IGME, Madrid, scale 1:50,000.

Odonne, F., 1987. Migrations de charnières et vecteurs de déplacements sur des modèles analogiques de plis superposés. Geodinamica Acta 1, 139–146.

Odonne, F., Vialon, P., 1987. Hinge migration as a mechanism of superposed folding. Journal of Structural Geology 9, 835–844.

Ramsay, J.G., 1967. Folding and Fracturing of Rocks. McGraw-Hill, New York.

Ramsay, J.G., Huber, M.I., 1987. The Techniques of Modern Structural Geology, Vol. 2: Folds and Fractures. Academic Press, London.

Roy, A.B., Sharma, B.L., Chauhan, N.K., 1998. Superposed buckle folding of garnet quartzite bands in phyllite of the Aravalli supergroup, northwest of Udaipur, Rajashtan. Indian Journal of Geology 70, 145–155.

Simón, J.L., 1980. Estructuras de superposición de plegamientos en el borde NE de la Cadena Ibérica. Acta Geológica Hispánica 15, 137–140.

Simón, J.L., 1984. Un faisceau de chevauchements induits par accidents du socle sur la bordure nord de la Chaîne Ibérique. Conference "Chevauchement et Déformation", Abstracts, Université de Toulouse, 46.

Simón, J.L., 1986. Analysis of a gradual change in stress regime (example from the eastern Iberian Chain, Spain). Tectonophysics 124, 37–53.

Simón, J.L., Arenas, C., Arlegui, L.E., Aurell, M., Gisbert, J., González, A., Liesa, C.L., Marín, C., Meléndez, A., Meléndez, G., Pardo, G., Soria, A.R., Soria, M., Soriano, M.A., 1998. Guía del Parque Geológico de Aliaga. Universidad de Zaragoza.

Simón, J.L., Liesa, C.L., Soria, A.R., 1999. Un sistema de fallas normales sinsedimentarias en las unidades de facies Urgon de Aliaga (Teruel, Cordillera Ibérica). Geogaceta 24, 291–294.

Skjernaa, L., 1975. Experiments on superposed buckle folding. Tectonophysics 27, 255–270.

Soria, A.R., 1997. La sedimentación en las cuencas marginales del surco Ibérico durante el Cretácico Inferior y su control estructural. Ph.D. thesis, Universidad de Zaragoza.

Stauffer, M.R., 1988. Fold interference structures and coaptation folds. Tectonophysics 149, 339–343.

Thiessen, R.L., Means, W.D., 1980. Classification of fold interference patterns: a reexamination. Journal of Structural Geology 2, 311–316.

Tobisch, O.T., 1967. The influence of early structures on the orientation of late-phase folds in an area of repeated deformation. Journal of Geology 75, 554–564.

Watkinson, A.J., 1981. Patterns of fold interference: influence of early fold shapes. Journal of Structural Geology 3, 19–23.